The Astrophysical Journal, 616:L11–L14, 2004 November 20

IMAGING THE DISK AROUND TW HYDRAE WITH THE SUBMILLIMETER ARRAY

Chunhua Qi,[1] Paul T. P. Ho,[1] David J. Wilner,[1] Shigehisa Takakuwa,[2] Naomi Hirano,[3] Nagayoshi Ohashi,[2,3] Tyler L. Bourke,[2] Qizhou Zhang,[1] Geoffrey A. Blake,[4] Michiel Hogerheijde,[5] Masao Saito,[2,6] Minho Choi,[3,7] and Ji Yang[8]

Received 2004 January 13; accepted 2004 March 17; published 2004 October 28

ABSTRACT

We present ~2″–4″ aperture synthesis observations of the circumstellar disk surrounding the nearby young star TW Hya in the CO $J = 2$–1 and $J = 3$–2 lines and associated dust continuum obtained with the partially completed Submillimeter Array. The extent and peak flux of the 230 and 345 GHz dust emission follow closely the predictions of the irradiated accretion disk model of Calvet et al. The resolved molecular line emission extends to a radius of at least 200 AU, the full extent of the disk visible in scattered light, and shows a clear pattern of Keplerian rotation. Comparison of the images with two-dimensional Monte Carlo models constrains the disk inclination angle to 7° ± 1°. The CO emission is optically thick in both lines, and the kinetic temperature in the line formation region is ~20 K. Substantial CO depletion, by an order of magnitude or more from canonical dark cloud values, is required to explain the characteristics of the line emission.

Subject headings: circumstellar matter — ISM: molecules — planetary systems: protoplanetary disks — radio lines: stars — stars: individual (TW Hydrae)

1. INTRODUCTION

TW Hya is the closest known classical T Tauri star and exhibits high X-ray flux, large lithium abundance, and evidence of an actively accreting disk with an accretion rate estimated to be from 10^{-9} to $10^{-8}\ M_\odot\ \mathrm{yr}^{-1}$ based on the large Hα equivalent width and the X-ray emission (Kastner et al. 2002 and references therein). Despite its apparently advanced age, estimated to be 5–20 Myr, TW Hya is surrounded by a disk of mass $\sim 5 \times 10^{-3}\ M_\odot$ inferred from dust emission (Wilner et al. 2000). The disk is viewed nearly face-on and is visible in scattered light to a radius of at least 3″.5, or 200 AU at a distance of 56 pc (Krist et al. 2000; Trilling et al. 2001; Weinberger et al. 2002; Calvet et al. 2002).

Several molecular species (CO, HCN, CN, HCO^+, DCO^+) have been detected in the TW Hya disk at millimeter and submillimeter wavelengths using single-dish telescopes (Kastner et al. 1997; van Zadelhoff et al. 2001; Thi et al. 2001; van Dishoeck et al. 2003). The proximity, isolation, and rich chemistry of the TW Hya disk make this system an excellent target for the study of the physical and chemical structure of protoplanetary environments at high spatial resolution using interferometry. Models may be directly compared to aperture synthesis images of molecular lines to verify the inferences from low-resolution observations and to further probe the kinematics, physical conditions, and chemistry. A first step in this direction was the imaging analysis of HCO^+ $J = 1$–0 emission observed with the Australia Telescope Compact Array by Wilner et al. (2003), although the spatial and spectral resolutions were insufficient to examine the kinematics in any detail.

The prospects are excellent for interferometric observations of protoplanetary disks at submillimeter wavelengths (Blake 2003). The Submillimeter Array (SMA),[9] now nearing completion on Mauna Kea, is an ideal instrument for making these observations (Ho et al. 2004). In this Letter, we present early SMA observations of the TW Hya disk in the CO $J = 3$–2 and $J = 2$–1 lines and dust continuum, with a maximum resolution of 2″. The resulting images unambiguously reveal the rotation of the disk around the star and constrain the disk inclination and size.

2. OBSERVATIONS

The SMA observations of TW Hya were made between 2003 March and June using two configurations of five of the 6 m diameter antennas at each of two frequencies (230 and 345 GHz). These observations provided 17 independent baselines ranging in length from 16 to 120 m. Table 1 summarizes the observational parameters. The synthesized beam sizes were ~2″ at 345 GHz and ~4″ at 230 GHz with robust weighting. The SMA digital correlator was configured with both a narrow band of 512 channels over 104 MHz, which provided 0.2 MHz frequency resolution (or 0.18 km s^{-1} velocity resolution at 345 GHz) and several broader bands that provided 656 MHz of bandwidth for continuum measurements. Calibration of the visibility phases and amplitudes was achieved with observations of the quasar 3C 273, typically at intervals of 30 minutes. Two weaker quasars closer to TW Hya on the sky, 1058+015 and 1037−295, were also observed to verify the effectiveness of phase referencing between 3C 273 and TW Hya. Observations of Callisto provided the absolute scale for the flux density calibration. The uncertainties in the flux scale are estimated to be 20% based on the scatter of the measurements on different days, which is due to the un-

[1] Harvard-Smithsonian Center for Astrophysics, 60 Garden Street, MS 42, Cambridge, MA 02138; cqi@cfa.harvard.edu.
[2] Harvard-Smithsonian Center for Astrophysics, Submillimeter Array Project, 645 North A'ohoku Place, Hilo, HI 96720.
[3] Academia Sinica Institute of Astronomy and Astrophysics, P.O. Box 23-141, Taipei 106, Taiwan.
[4] Divisions of Geological and Planetary Sciences and Chemistry and Chemical Engineering, California Institute of Technology, MS 150-21, Pasadena, CA 91125.
[5] Sterrewacht Leiden, P.O. Box 9513, 2300 RA Leiden, Netherlands.
[6] National Astronomical Observatory of Japan, 2-21-1 Osawa, Mitaka, Tokyo 181-8588, Japan.
[7] Taeduk Radio Astronomy Observatory, Korea Astronomy Observatory, Hwaam 61-1, Yuseong, Daejeon 305-348, Korea.
[8] Purple Mountain Observatory, Chinese Academy of Sciences, Nanjing 21008, China.

[9] The Submillimeter Array is a joint project between the Smithsonian Astrophysical Observatory and the Academia Sinica Institute of Astronomy and Astrophysics, and is funded by the Smithsonian Institution and the Academia Sinica.

TABLE 1
OBSERVATIONAL PARAMETERS FOR SMA TW HYA

Parameter	CO (3–2)	CO (2–1)
Rest frequency (GHz)	345.796	230.538
Observations (2003)	Mar 15, Apr 21	Mar 24, Apr 20, May 3
Synthesized beam	2.″9 × 2.″1 (P.A. = 3.°4)	4.″7 × 2.″7 (P.A. = 9.°9)
rms[a] (continuum; mJy beam^{-1})	35	6.8
Dust flux (Jy)	1.46 ± 0.04	0.57 ± 0.02
Channel spacing (km s^{-1})	0.18	0.26
rms[a] (line; Jy beam^{-1})	1.1	0.28
Integrated intensity (K km s^{-1})	23.7	10.6
Peak intensity (K)	25.9	14.7
ΔV[b] (km s^{-1})	0.86 ± 0.02	0.73 ± 0.02

[a] Signal-to-noise ratio limited by the dynamic range.
[b] Based on Gaussian fits to the spectra (FWHM).

certainties in pointing models and system temperature measurements. The data were calibrated using the MIR software package adapted for the SMA from the IDL version of the MMA software package developed originally for the Owens Valley Radio Observatory (Scoville et al. 1993). The continuum emission from TW Hya is strong enough for self-calibration, and an iteration of phase-only self-calibration was performed to improve the images by 20%. The NRAO AIPS package was used to generate continuum and spectral line images, all of which were CLEANed in the usual way.

3. RESULTS

3.1. *Continuum Emission*

Calvet et al. (2002) have developed a physically self-consistent irradiated accretion disk model for TW Hya. This unique model requires a distinct transition in disk properties at a radius of ≈4 AU, likely due to a developing gap, and grains that have grown to sizes of ≈1–10 cm in order to match the full spectral energy distribution (SED) from optical to radio wavelengths. The Calvet et al. model is consistent with the radial brightness distribution of the disk observed at 43 GHz, where the dust emission has been resolved by the VLA (Wilner et al. 2000). The new SMA continuum measurements agree well with previous single-dish observations at these wavelengths and with the predictions of the Calvet et al. model. To compare the dust emission to the model radial brightness, we show in Figure 1 the visibility amplitudes at 345 GHz, annularly averaged in 20 kλ bins, with the model curve (scaled by 0.9, well within the uncertainties of the flux scale). The good match of the SMA continuum measurements with previous data and with the irradiated accretion disk model predictions gives us confidence in the reliability of the submillimeter measurements as well as the accuracy of the absolute flux scale.

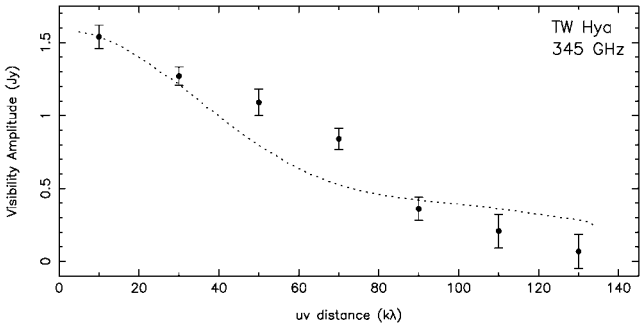

FIG. 1.—Visibility amplitudes of the observed and modeled 345 GHz continuum emission from TW Hya, annularly averaged in 20 kλ bins. The error bars represent ±1 σ for each bin. The curve shows the visibility amplitudes derived from the model calculations of Calvet et al. (2002) of an irradiated accretion disk, which fits the full SED well after applying an amplitude scale factor of 0.9.

3.2. CO $J = 2$–1 *and* $J = 3$–2 *Emission*

Figure 2 shows spectra of the CO $J = 2$–1 and $J = 3$–2 line emission at the TW Hya continuum peak. Both lines are detected with high signal-to-noise ratios. The CO emission from the disk is spatially resolved; a circular Gaussian fit to the CO (3–2) integrated intensity map gives an FWHM size of 3.″5 ± 0.″3. Table 1 lists the integrated intensities and results of Gaussian fits to the central spectra. As indicated by Beckwith & Sargent (1993) and van Zadelhoff et al. (2001), CO $J = 2$–1 and CO $J = 3$–2 emission are expected to be highly optically thick in circumstellar disks. These lines are thus excellent probes of the outer disk velocity field but do not robustly trace the disk mass (Simon et al. 2000; Qi et al. 2003). Furthermore, the peak intensities should be tied to the kinetic temperatures of the regions of the disk where the lines become optically thick, and as TW Hya appears almost face-on, any differences in brightness may be related to vertical temperature gradients.

Comparing the intensities of the two transitions within the same region (here the CO $J = 3$–2 data set is convolved with the CO

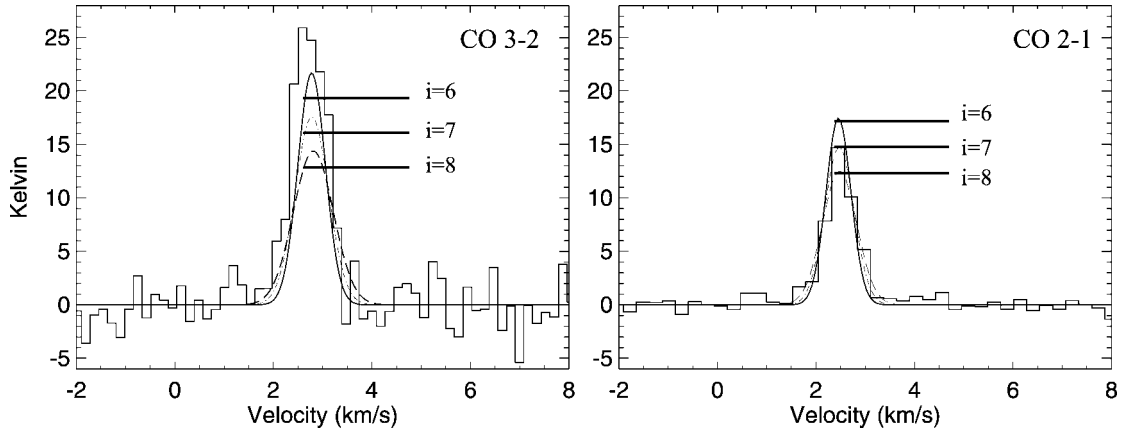

FIG. 2.—CO $J = 3$–2 and $J = 2$–1 spectra at the continuum (stellar) position; the beam sizes are listed in Table 1. The curves show synthetic spectra for a small range of inclination angles using the model parameters listed in Table 2.

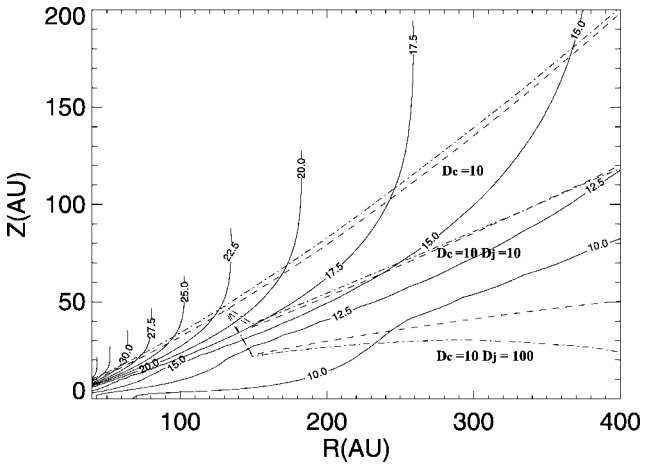

FIG. 3.—Gas kinetic temperature from the TW Hya model of Calvet et al. (2002; *solid lines*) and the $\tau = 1$ surfaces for the CO $J = 3$–2 and $J = 2$–1 lines for the three depletion scenarios described in the text (*dashed and dot-dashed lines*).

$J = 2$–1 beam), the peak brightness of the CO $J = 3$–2 line is 21.0 ± 0.7 K, and that of the CO $J = 2$–1 line is 14.7 ± 0.4 K. Figure 3 shows the location of the $\tau = 1$ surfaces for these CO transitions calculated together with contours from the kinetic temperature model of Calvet et al. (2002) for three different depletion scenarios. All assume a constant depletion factor (D_c) of 10. The top set is calculated with the constant D_c, the one below includes additional jump depletion (D_j) by a factor of 10 in which the kinetic temperature falls below 22 K (the critical temperature of CO desorption; van Zadelhoff et al. 2001), and the bottom one includes D_j of 100 at that same temperature threshold. For the first case, the temperature gradient probed by the two CO lines is very small, as both transitions are formed at nearly the same location in the disk. In the case in which D_j is 10, however, the $\tau = 1$ surfaces for both transitions show an abrupt change near 130–150 AU in radius and 20–40 AU in height. With an even larger D_j of 100, the CO $J = 3$–2 line becomes optically thick significantly deeper (colder) in the disk than does the CO $J = 2$–1 line in the region beyond 200 AU where the temperature is very low. The T_B of CO (3–2) is predicted to be smaller than that of CO (2–1) in this case, which is not compatible with the SMA spectra reported here.

The observed difference in the brightness temperatures of the CO lines in Figure 2 must therefore arise from a combination of factors. The beam size for the CO $J = 3$–2 spectrum corresponds to ~160 × 120 AU (FWHM), and that for CO $J = 2$–1 corresponds to ~260 × 150 AU (FWHM). Both zones have a $\tau = 1$ surface above 22 K, although the CO $J = 2$–1 data do sample colder regions where the $\tau = 1$ surface drops to less than 20 K. The velocity-integrated intensities for the full disk in the two CO lines are 37.2 ± 7.5 Jy km s^{-1} for CO $J = 3$–2 and 12.4 ± 1.0 Jy km s^{-1} for CO $J = 2$–1, as compared to previous single-dish observations of 36.6 Jy km s^{-1} for CO $J = 3$–2 (van Zadelhoff et al. 2001) and 17.7 Jy km s^{-1} for CO $J = 2$–1 (Kastner et al. 1997). We regard these as consistent given the uncertainties in the flux scales of the various telescopes. The ratio of integrated intensities from the aggregate 345 GHz/230 GHz data sets is 2.45 ± 0.6, consistent with the value of 2.25 expected if the lines were optically thick and tracing isothermal gas. As mentioned above, even with the same convolving beam, the CO $J = 3$–2 emission remains brighter than that from CO $J = 2$–1 (21 K vs. 15 K). Figure 2 shows that there is likely to be a small vertical temperature gradient to which these two transitions can be quite sensitive, e.g., for the case of an inclination angle of 7° where CO $J = 2$–1 traces gas near ~15 K, while the more optically thick CO $J = 3$–2 emission arises from gas closer to the disk surface and therefore somewhat warmer (~18 K). Given the likely flux uncertainties of the SMA and single-dish observations, it is difficult at present to quantify whether vertical temperature gradients in the disk or beam dilution dominate the observed difference in the brightness temperatures of the CO lines shown in Figure 2. Studies of additional CO transitions and, especially, isotopically substituted variants could settle this issue definitively.

Figure 4 (*upper panels*) shows a set of velocity channel maps for 0.18 km s^{-1} intervals for the CO $J = 3$–2 line. The main feature of interest is the position shift along a northwest-southeast axis at velocities that bracket the systemic velocity. In order to interpret these images in a quantitative way, we use a two-dimensional accelerated Monte Carlo model (Hogerheijde & van der Tak 2000) to calculate the radiative transfer and molecular excitation. We adopt the physical density and temperature structure derived by Calvet et al. (2002), which does an excellent job reproducing the dust continuum emission, and we produce a grid of models with a range of inclinations and various depletion schemes to simulate the disk as imaged by a telescope with the resolution constrained only by the grid sampling (typically this is of order 5–10 AU in the outer disk, or 0.″1–0.″2). Simulated observations of the model disks were produced by the MIRIAD software package using the UVMODEL routine to select synthetic visibility observations at the observed (u, v)-spacings. These synthetic visibilities were then processed into images in a manner identical to the SMA data for detailed comparisons (more detailed explanations and a description of the model may be found in Kessler 2003; for an application to LkCa 15, see Qi et al. 2003).

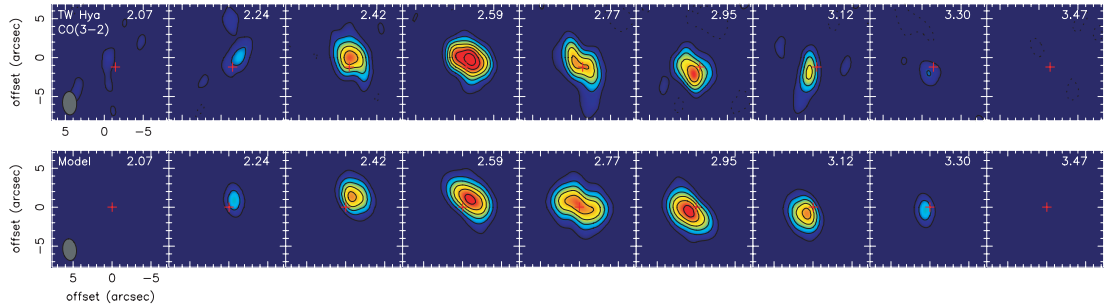

FIG. 4.—SMA images of the CO $J = 3$–2 emission from TW Hya in 0.18 km s^{-1} velocity bins observed with the SMA (*upper panels*, with a contour spacing of 5 Jy beam^{-1}) together with images from a simulated observation using the model parameters listed in Table 2 (*lower panels*, with a contour spacing of 3 Jy beam^{-1}). The small cross indicates the position of the continuum source.

The CO data provide a strong constraint on the disk inclination i or, more specifically, sin i. Previous analyses of scattered light images (Krist et al. 2000; Trilling et al. 2001) indicated that TW Hya and its disk are seen close to pole-on, but the inclination angle could not be well constrained. For the disk models used here, we fix the inner radius at 4 AU and the outer radius at 196 AU, and we adopt Keplerian rotation along with a low turbulent velocity of 0.05 km s^{-1} through comparison to the observed CO $J = 3$–2 and $J = 2$–1 line profiles. Indeed, turbulent velocities in the outer disk also affect the line width, but values of $\geq$0.1 km s^{-1} or larger cannot reproduce the peanut-shaped morphology of the systemic velocity channel map while the line widths are essentially unchanged for turbulent velocities in the 0.05–0.1 km s^{-1} range. Figure 2 shows the predictions for a range of inclination angles, which strongly impact the widths of the lines; the best-fit inclination is 7°, which is slightly larger than the inclination angle of 4° derived from the ellipticity of the infrared image of the disk around TW Hya in scattered light (Weinberger et al. 2002) where a circular disk is assumed. Specifically, the predicted line widths change by 30%, from 0.72 to 1.06 km s^{-1} for CO $J = 3$–2 and from 0.6 to 0.85 km s^{-1} for CO $J = 2$–1, as the inclination angles vary from 6° to 8°. Such significant line width variations with inclination angle (by as little as 1°) are expected when the disk is so close to pole-on because the loci of constant projected velocities are quite sensitive to sin i—the error of which translates to a very tight limit on i. An inclination angle of 7° $\pm$ 1° is thus a robust fit that is strongly constrained by the CO line widths within the confines of the disk model employed. In general, the derived inclination angle can also be coupled to the size of the disk and the radial and vertical temperature gradients. The line intensity of CO (3–2) is still much larger than the model prediction, suggesting that the near-surface gas temperature in the Calvet et al. model is somewhat too low. The line profiles are also not perfectly characterized as Gaussian (although they are very narrow), but we rely on them for determining the line widths. Each of these systematic uncertainties could be larger than the uncertainty of the inclination angle (1°) that we determine from the line widths but can be constrained in the future by higher spatial resolution observations of additional CO transitions and isotopologues.

A comparison of the observed channel maps of CO $J = 3$–2 and the synthetic maps generated by a detailed model with parameters listed in Table 2 is shown in Figure 4. While the model reproduces all of the major features observed, in particular the velocity gradient and peanut-shaped morphology of the central channel, the predicted CO (3–2) intensities in Figures 2 and 4 are 40% smaller than observed. It is likely that the vertical gas and dust temperature gradient difference is not quite captured by the SED-constrained disk models, which we will pursue further in a future paper. Resolved observations of CO isotopologues toward another T Tauri star, DM Tau, have been presented by Dartois et al. (2003), who used IRAM inteferometric data to constrain the depletion and temperature versus radius, as the less abundant species probe the inner part of the disk, within an LTE excitation/radiative transfer model. Such an approach is useful for molecules such as CO that possess low critical densities, but as has been discussed by van Zadelhoff et al. (2003), LTE excitation is not a good approximation for higher dipole moment species such as CN. With the two-dimensional Monte Carlo model, the statistical nature of the molecular excitation can be investigated within the context of realistic models of the disk structure. Chemical differentiation can therefore be constrained by resolved observations of multiple transitions of species with varying characteristics, and our future publications will thus include studies of other molecules, including CN and HCN, toward TW Hya.

TABLE 2
Model Parameters Used in Simulating TW Hya CO Emission

Parameter	Value
Physical structure	Irradiated accretion disk[a]
Stellar mass ($M_\odot$)	0.6
Disk size (AU)	$R_{in} = 4$, $R_{out,\,edge} = 196$
Disk P.A. (deg)	−45
Inclination angle (deg)	7
Turbulent velocity (km s^{-1})	0.05
Depletion factor (K)	10 × (100 × for $T \leq 22$)

[a] Calvet et al. (2002).

We thank all the SMA staff members for their diligent work in completing the SMA. We also thank P. D'Alessio and N. Calvet for providing the disk model of TW Hya and J. E. Kessler-Silacci for helpful discussions concerning the radiative transfer model. And we are grateful to J. H. Kastner for useful comments.

REFERENCES

Beckwith, S. V. W., & Sargent, A. I. 1993, in Protostars and Planets III, ed. E. H. Levy, J. I. Lunine, & M. S. Matthews (Tucson: Univ. Arizona Press, 521
Blake, G. A. 2003, in Chemistry as a Diagnostic of Star Formation, ed. C. L. Curry & M. Fich (Ottawa: NRC Res. Press), 178
Calvet, N., D'Alessio, P., Hartmann, L., Wilner, D., Walsh, A., & Sitko, M. 2002, ApJ, 568, 1008
Dartois, E., Dutrey, A., & Guilloteau, S. 2003, A&A, 399, 773
Ho, P., Moran, J. M., & Lo, K. Y. 2004, ApJ, 616, L1
Hogerheijde, M. R., & van der Tak, F. F. S. 2000, A&A, 362, 697
Kastner, J. H., Huenemoerder, D. P., Schulz, N. S., Canizares, C. R., & Weintraub, D. A. 2002, ApJ, 567, 434
Kastner, J. H., Zuckerman, B., Weintraub, D. A., & Forveille, T. 1997, Science, 277, 67
Kessler, J. E. 2003, Ph.D. thesis, Caltech
Krist, J. E., Stapelfeldt, K. R., Ménard, F., Padgett, D. L., & Burrows, C. J. 2000, ApJ, 538, 793
Qi, C., Kessler, J. E., Koerner, D. W., Sargent, A. I., & Blake, G. A. 2003, ApJ, 597, 986
Scoville, N. Z., Carlstrom, J. E., Chandler, C. J., Phillips, J. A., Scott, S. L., Tilanus, R. P. J., & Wang, Z. 1993, PASP, 105, 1482
Simon, M., Dutrey, A., & Guilloteau, S. 2000, ApJ, 545, 1034
Thi, W. F., et al. 2001, ApJ, 561, 1074
Trilling, D. E., Koerner, D. W., Barnes, J. W., Ftaclas, C., & Brown, R. H. 2001, ApJ, 552, L151
van Dishoeck, E. F., Thi, W.-F., & van Zadelhoff, G.-J. 2003, A&A, 400, L1
van Zadelhoff, G.-J., Aikawa, Y., Hogerheijde, M. R., & van Dishoeck, E. F. 2003, A&A, 397, 789
van Zadelhoff, G.-J., van Dishoeck, E. F., Thi, W.-F., & Blake, G. A. 2001, A&A, 377, 566
Weinberger, A. J., et al. 2002, ApJ, 566, 409
Wilner, D. J., Bourke, T. L., Wright, C. M., Jørgensen, J. K., van Dishoeck, E. F., & Wong, T. 2003, ApJ, 596, 597
Wilner, D. J., Ho, P. T. P., Kastner, J. H., & Rodríguez, L. F. 2000, ApJ, 534, L101